Multimodal Imaging Evidence for a Frontocortical Modulation of Visual Cortex during the Selective Processing of Conditioned Threat*

Nathan M. Petro[1], L. Forest Gruss[1], Siyang Yin[1], Haiqing Huang[1], Vladimir Miskovic[2], Mingzhou Ding[1], and Andreas Keil[1]

Abstract

■ Emotionally salient cues are detected more readily, remembered better, and evoke greater visual cortical responses compared with neutral stimuli. The current study used concurrent EEG-fMRI recordings to identify large-scale network interactions involved in the amplification of visual cortical activity when viewing aversively conditioned cues. To generate a continuous neural signal from pericalcarine visual cortex, we presented rhythmic (10/sec) phase-reversing gratings, the orientation of which predicted the presence (CS+) or absence (CS−) of a cutaneous electric shock (i.e., the unconditioned stimulus). The resulting single trial steady-state visual evoked potential (ssVEP) amplitude was regressed against the whole-brain BOLD signal, resulting in a measure of ssVEP-BOLD coupling. Across all trial types, ssVEP-BOLD coupling was observed in both primary and extended visual cortical regions, the rolandic operculum, as well as the thalamus and bilateral hippocampus. For CS+ relative to CS− trials during the conditioning phase, BOLD-alone analyses showed CS+ enhancement at the occipital pole, superior temporal sulci, and the anterior insula bilaterally, whereas ssVEP-BOLD coupling was greater in the pericalcarine cortex, inferior parietal cortex, and middle frontal gyrus. Dynamic causal modeling analyses supported connectivity models in which heightened activity in pericalcarine cortex for threat (CS+) arises from cortico-cortical top–down modulation, specifically from the middle frontal gyrus. No evidence was observed for selective pericalcarine modulation by deep cortical structures such as the amygdala or anterior insula, suggesting that the heightened engagement of pericalcarine cortex for threat stimuli is mediated by cortical structures that constitute key nodes of canonical attention networks. ■

INTRODUCTION

An organism's survival depends on its ability to quickly and adaptively respond to environmental challenges and opportunities. To accomplish this task, the mammalian brain detects and stores the predictive value of recurring environmental signals with respect to dangerous or rewarding outcomes (Sokolov, 1963). This process results in the formation of associative memories that are thought to be implemented in distributed brain networks encompassing cortical as well as subcortical structures (Linnman, Rougemont-Bucking, Beucke, Zeffiro, & Milad, 2011). In complex and uncertain environments, associative learning depends on the organism's ability to correctly select the relevant sensory cues from the environmental noise (Headley & Weinberger, 2011; Mayr, 1974). Thus, established associative networks that link specific stimuli to representations of biological significance and motor action are hypothesized to possess strengthened sensory representations (Mirabella et al., 2007; Gallant, Connor, & Van Essen, 1998). Supporting this notion, visual and auditory stimuli representing motivationally relevant contexts, such as pictures of bodily injury or the voice of a crying infant, prompt relatively larger responses in sensory cortical areas of the human brain (reviewed in Sabatinelli et al., 2011). An extensive literature has demonstrated that the neural and hemodynamic amplification of threat, relative to neutral, cues is paralleled by a host of behavioral effects such as facilitated detection (Öhman & Soares, 1998), identification (Anderson, 2005), and greater perceptual vividness (Todd & Thompson, 2015). The question arises regarding the neurophysiological mechanisms mediating such differences in sensory and perceptual processing. Research using rodent models has established many microscopic and molecular mechanisms mediating responses to threat cues in evolutionary old structures such as the amygdala (Sears, Schiff, & LeDoux, 2014; Amaral, Behniea, & Kelly, 2003; Clugnet & LeDoux, 1990). Similarly, previous studies using hemodynamic neuroimaging in humans have highlighted the role of amygdaloid and frontal cortical regions during emotional processing, including responses to aversive stimuli (e.g., Furl, Henson, Friston, & Calder, 2013). What is not known is how brain regions interact to enable the selectively facilitated visual processing of threat—one of the first stages in the sequence of adaptive behaviors prompted by the onset of an aversive stimulus (Sokolov, 1963).

[1]University of Florida, [2]SUNY Binghamton

*Affective-Motivational Salience and Attentional Sets Special Focus: This paper was presented at the Cognitive Neuroscience Society Meeting, New York City, April 2016.

Journal of Cognitive Neuroscience 29:6, pp. 953–967
doi:10.1162/jocn_a_01114

The current study addressed this problem by quantifying the large-scale neurophysiological changes measured by concurrent EEG-fMRI recordings, as observers learned that an initially neutral visual stimulus comes to predict an aversive outcome. In differential aversive conditioning, one of two initially innocuous stimuli (conditioned stimuli [CS]) gains motivational relevance through reliably predicting the occurrence (CS+) of a noxious event (the unconditioned stimulus [US]), whereas the other stimulus (CS−) predicts its absence. Previous work in the animal model and in human observers suggests that aversive conditioning with a specific sensory feature results in retuning of sensory cortical receptive fields, amplifying the cortical representation of the CS+, compared with the CS− (Stolarova, Keil, & Moratti, 2006; Weinberger, 2004). One prevalent hypothesis holds that this sensory amplification of threat cues is driven by the amygdaloid complex that is thought to provide reentrant bias signals to neurons along the ventral visual stream (Delgado, Olsson & Phelps, 2006; Amaral, 2003). This hypothesis has recently been challenged, for example, by the finding that visual amplification of threat cues is seen in participants with amygdala resection (Edmiston et al., 2013). Human neuroimaging research has suggested several further candidate structures that may be involved in the reentrant modulation of visual cortex during threat processing. Meta-analyses suggest the co-occurrence of selective BOLD enhancement not only in the visual cortex but across a set of functionally connected brain regions such as the dorsal ACC, the anterior insular cortex, and OFC (see Fullana et al., 2016, for a recent review). Previous analyses of network activity during aversive conditioning using fMRI have considered voxel-wise correlations across the entire BOLD time series during habituation, acquisition, and extinction. This procedure is robust, intuitive, and valid but does not allow the separate quantification of connectivity for the CS+ and CS− trials, which are typically intermixed. Comparing acquisition and habituation phases, these studies have reported that functional networks emerge that involve the hippocampus, anterior insula, and ACC (Linnman et al., 2011), as well as heightened covariation among primary and extended visual cortices (Damaraju, Huang, Barrett, & Pessoa, 2009). Furthermore, electric and magnetic brain recordings in humans have suggested that cortico-cortical interactions between visual areas and frontoparietal cortices mediate the heightened visual responses to threat seen at the behavioral and neural levels (Miskovic & Keil, 2014; Keil et al., 2009; Moratti, Keil, & Stolarova, 2004). These studies, however, were limited by the low spatial specificity of scalp-recorded measures of brain activity. Here, we use multimodal imaging to test the hypothesis that threat cue facilitation in human visual cortex is mediated by selective top–down bias signals originating in anterior cortical structures.

This study leveraged the excellent temporal and spatial resolution of combined EEG-fMRI recordings by evoking a robust visual electrocortical signal, the steady-state visual evoked potential (ssVEP). The ssVEP is evoked by the periodic modulation of a visual stimulus in terms of luminance or contrast. It can be extracted from scalp-recorded EEG and reflects postsynaptic neural population activity that primarily originates in pericalcarine regions of the visual cortex (Di Russo et al., 2007). The ssVEP amplitude is enhanced when neutral visual cues acquire aversive value during classical conditioning (McTeague, Gruss, & Keil, 2015; Miskovic & Keil, 2012). For the present set of analyses, a key advantage of ssVEPs is that they can be reliably measured at the level of single trials (Keil et al., 2008) and are therefore well suited for revealing trial-by-trial coupling between the pericalcarine cortex and whole-brain BOLD signals. The goal of quantifying the covariation of this spatially specific electrophysiological index with hemodynamic (BOLD) data is to identify brain regions that are temporally coupled with visual cortex over the course of the aversive conditioning paradigm. The rationale is that regions displaying such temporal coupling may be involved in the hypothesized bidirectional interactions mediating facilitated visual processing of conditioned threat cues.

In addition to seeking converging evidence of BOLD-alone analyses with the ssVEP-BOLD results, we also tested the connectivity of candidate structures arising from ssVEP-BOLD analyses, using dynamic causal modeling (DCM). DCM enables testing models regarding the modulatory influence of extravisual signals into pericalcarine visual cortex that mediate the heightened visual processing of threat cues. Overall, this approach allowed us to test the hypotheses that emerging perceptual biases to learned threat cues—measured by changes in ssVEP amplitude—are accompanied by commensurate BOLD changes in anterior regions of the brain and that these regions are the origin of modulatory top–down signals, selectively amplifying the visual cortical response to threat.

METHODS

Participants

Participants consisted of 15 (5 women; age: mean = 21.73 years, *SD* = 3.43 years) students who, after giving written informed consent, participated on a volunteer basis or received course credit for the General Psychology course at the University of Florida. All participants were screened for ferromagnetic implants, claustrophobia, and personal or family history of epilepsy or photic seizures. Female participants self-administered a pregnancy test before participation. Data of three additional participants were discarded because of excessive EEG artifact. All procedures were approved by the institutional review board of the University of Florida and were consistent with the Declaration of Helsinki on studies with human participants.

Stimuli and Experimental Design

Stimuli consisted of sinusoidal gratings multiplied with a Gaussian envelope (i.e., Gabor patches) oriented at

either 15° or 345° relative to the vertical meridian, which reversed their phase every 100 msec to evoke an ssVEP having its second harmonic at 10 Hz. Consistent with previous studies of phase reversal ssVEP (Keil, Miskovic, Gray, & Martinovic, 2013; see Norcia, Appelbaum, Ales, Cottereau, & Rossion, 2015, for a review), we analyzed the second harmonic response, that is, 10 Hz. Gabor patches had a maximum Michelson contrast of 95% (maximum = 110 cd/m^2; minimum = 2.1 cd/m^2) and a spatial frequency of 0.45 cycles per degree. Gratings were presented at a horizontal visual angle of 15.5°, respectively, on an MR-compatible monitor placed outside the scanner bore, which participants viewed via a mirror placed on the MR head coil positioned 8.5 cm from the eyes. All visual stimuli were presented on a black background (1.2 cd/m^2). The gratings were used as CS during the classical differential conditioning design in which their orientation predicted the presence (CS+) or absence (CS−) of a US in the form of a cutaneous electric shock. The US was administered to the participant's right ankle for a duration of 0.5 msec beginning at the start of the final phase reversal cycle of the grating at an intensity determined by a build-up procedure (see below) conducted before entering the scanner environment. All stimulus presentation was controlled using E-Prime software (Psychology Software Tools, Pittsburgh, PA). Cutaneous shocks were administered using an STMISO Stimulation Isolation Adapter (BIOPAC Systems, Inc., Goleta, CA) with MRI-compatible skin electrodes.

Each trial consisted of one of the two gratings being presented for 5100 msec, during which its phase was alternated every 100 msec. For the CS+–US paired trials (see below), an additional reversal cycle (200 msec) was appended to the end of the phase reversal train to account for the US presentation. This ensured overlap of CS+ and US, as is characteristic for classical conditioning. An intertrial interval consisted of an initial gray cross (37.5 cd/m^2; 1° of visual angle) presented in the middle of the screen for a random duration between 0 and 8 sec followed by a white cross (149.0 cd/m^2) for a duration of 3 sec, immediately preceding trial onset with Gabor patch presentation.

The experiment consisted of 129 trials in total, across three experimental blocks: 40 habituation, 49 acquisition, and 40 extinction trials. For the habituation and extinction blocks, CS+ and CS− trials were presented for 20 trials each in pseudorandom order. For the acquisition block, CS− trials were presented 20 times whereas CS+ trials occurred 29 times. Among CS+ trials during this acquisition block, the US was presented on nine trials consisting of four initial CS+ trials and five of the remaining 25 CS+ trials (following a 25% reinforcement schedule), dispersed pseudorandomly. These nine CS+–US paired trials were discarded from all subsequent BOLD analyses to avoid including BOLD changes related to somatosensory activity in subsequent contrasts, leaving 40 trials for all analyses.

Procedure

Two electrodes were placed on the participant's right ankle for shock administration. Participants then underwent a brief build-up procedure, in which the shock was presented in steps of increasing intensity until the intensity reached a level of being "unpleasant, but not painful." This intensity was used during the experiment.

Participants were instructed to remain still while in the scanner and to maintain fixation on the center of the screen during all parts of the experiment. For the habituation block, participants were instructed that they would not feel a shock but to watch the patterns as they were presented. During the acquisition block, participants were informed that they would intermittently feel a shock during the course of the experiment but were not given indication as to any contingency between Gabor patch orientation and shock administration. The extinction block was also uninstructed, such that participants were given no indication as to whether or not they would feel a shock.

SAM Ratings

At the conclusion of the experiment, participants rated the CS and US on valence and arousal using the Self-Assessment Manikin (SAM; Bradley & Lang, 1994). These ratings were used to determine whether differences between the CS+ and CS− were seen after the extinction phase of the experiment, in terms of self-reported affect. Ratings of emotional arousal and hedonic valence for the CS+ and CS− visual gratings were compared using a paired-sample t test.

EEG Recording and Data Reduction

EEG data were recorded on a 32-channel MR-compatible system (Brain Products, München, Germany) during simultaneous BOLD acquisition (see below). This EEG system consisted of 31 Ag/AgCl electrodes placed on the head according to the 10–20 system and one electrocardiogram (EKG) electrode placed on the upper back to record heartbeats. Electrode FCz was used as the reference during recording. Impedances were kept below 20 kΩ for all scalp electrodes and below 50 kΩ for the EKG electrode, as suggested by the Brain Products manual. EEG data were digitized at 16-bit resolution using a sample rate of 5 kHz with a 0.1–250 Hz (3 dB point) bandpass filter applied online (Butterworth, 18 dB/octave roll off). A fiber-optic cable transferred the digitized data to the computer. The system was synchronized to the internal clock of the scanner.

The Brain Vision Analyzer 2.0 (Brain Products) software was used to remove artifacts caused by the magnetic gradients and heartbeats. Removal of magnetic gradient artifacts followed a modified version of the algorithm developed in Allen, Josephs, and Turner (2000), in which an artifact template constructed from a sliding window of

41 consecutive volumes is subtracted from the EEG data according to the event markers sent from the scanner's internal clock. Cardioballistic artifacts were removed using an algorithm developed by Allen, Polizzi, Krakow, Fish, and Lemieux (1998). This method detected *R* peaks in the CB electrode and created a template from 21 consecutive heartbeats, which was subtracted from the continuous EEG data. Data were then down-sampled to 250 Hz for computational efficiency and exported to EEGLab (Delorme & Makeig, 2004). A 5–15 Hz band-pass Kaiser filter implemented in EEGLab was applied to the continuous data. Following the filter, the EEG data were segmented from −400 to 5200 msec relative to the onset of the Gabor patch. No additional artifact rejection was performed after this point; however, technical failure resulted in the loss of 10 trials for one participant and 2 trials for another participant during the habituation phase only. All remaining EEG data were used in the subsequent data processing pipeline as described below.

Single-trial ssVEP Estimation

The EEG signal averaged across all participants and trials at sensor Oz is shown in Figure 1 (bottom), for which the maximum amplitude in the frequency domain matches the ssVEP stimulation frequency of 10 Hz (Figure 1, top). Estimates of single-trial 10 Hz evoked oscillatory activity were extracted using a moving window average (Keil et al., 2008). To avoid ERP contamination, a 964–4964 msec postonset segment of each epoch was used in this process. For each trial, a 400-msec time window was shifted across this time segment in steps of 100 msec and the contents of the window averaged, resulting in a 400-msec segment containing four cycles of the ssVEP and representing an average of 36 sliding windows. These averages were transformed into the frequency domain using a discrete Fourier transform (DFT). The 400 msec window resulted in a spectrum with a frequency resolution of 2.5 Hz. Following extraction of the amplitude spectrum (by computing the magnitude of the complex Fourier coefficients at each frequency), the spectrum was normalized by the number of frequency bins. The ssVEP amplitude was then extracted as the spectral amplitude at the 10-Hz driving frequency, and amplitude at sensor Oz was used for subsequent statistical analyses.

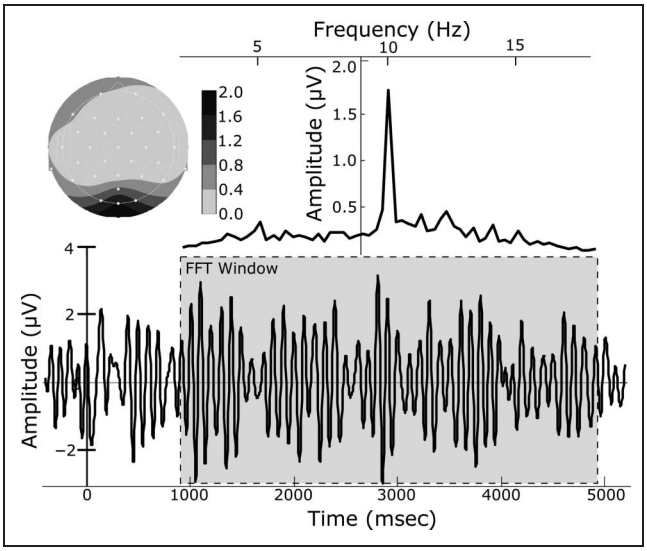

Figure 1. Time series of the filtered (5–15 Hz) EEG for one representative subject, averaged over all trials and segmented relative to onset of the Gabor patch which alternated at 10 Hz, evoking the ssVEP (bottom). This 10-Hz oscillation is the dominant signal as illustrated by the frequency domain data (top right) and is strongest over sensor Oz (top left), achieved by a Fourier transformation on a 4000-msec segment of EEG data (bottom, gray box).

To assess the reliability of single-trial ssVEP amplitude estimates, values at Oz were submitted to a Cronbach's (Cronbach, 1947) test of internal consistency using trials as observations. This test yielded a Cronbach's alpha of >.90 across the electrode array and an alpha of .94 at Oz, indicating a high degree of internal consistency among ssVEP values across participants.

ssVEP Analysis

For both CS conditions separately, estimates of single-trial ssVEP amplitude at sensor Oz were averaged across three experimental phases representative of the learning process implemented in our experimental design, which consisted of (1) preconditioning, (2) postconditioning, and (3) postextinction. The preconditioning phase consisted of the whole habituation block. On the basis of a body of previous ssVEP and heart rate (HR) studies of classical aversive conditioning (e.g., Wieser et al., 2014; Moratti & Keil, 2005), the second phase consisted of the whole acquisition block as well as the first half of the extinction block. Including the first half of extinction in the postacquisition phase ensured accurate representation of ssVEP changes occurring after the full acquisition phase, as observed previously in conditioning paradigms without explicit contingency instruction (Moratti, Keil, & Miller, 2006). On the basis of the same rationale, the second half of the extinction block was treated as a separate postextinction phase to reflect processes occurring after most observers had undergone fear extinction. After averaging, ssVEP amplitude values were log-transformed to reduce the amplification of between-subject differences associated with using spectral power data. For each experimental phase separately, a dependent samples *t* test was conducted between CS types.

Heart Rate Analysis

The EKG channel was used to calculate heart rate reactivity as the change from baseline in beats per minute (BPMs). To this end, data were segmented from −3000 to 7000 msec relative to the onset of the CS stimulus. R-waves were detected within each segment, allowing

computation of interbeat (R-R) intervals, and BPMs were determined by calculating weighted inverse values of interbeat intervals for 1-sec bins, as described by Graham (1978). Single-trial BPM waveforms were averaged together into the same three phases as described for the analysis of ssVEP amplitudes. Participant-averaged BPM time series were then baseline-corrected from −2000 to 1000 msec relative to stimulus onset. To assess heart rate deceleration, the minimum value from 0 to 3000 msec after stimulus onset was extracted for each participant, CS type, and experimental phase. For each experimental phase separately, both CS types were submitted to a dependent samples t test.

BOLD Recording and Preprocessing

MRI data were collected on a 3-T Philips Achieva scanner. Functional volumes varied between 202 and 468 per experimental block and were acquired during gradient-echo EPI sequence (echo time = 30 msec, repetition time = 1.98 sec, flip angle = 80°, slice number = 36, field of view = 224 mm, voxel size = 3.5 × 3.5 × 3.5 mm, matrix size 64 × 64). The first four functional scans were discarded to allow for scanner stabilization. Slices were acquired in ascending order oriented parallel to the plane connecting the anterior and posterior commissure during a 1850-msec interval with 130 msec between each repetition time, during which no images were collected and which allowed for visual inspection of the EEG data during recording when the MR gradient artifact was absent. Structural scans were acquired from T1-weighted images acquired during a magnetization-prepared 180° radio-frequency pulse and rapid gradient-echo (MP RAGE) sampling sequence (echo time = 3.1 msec, repetition time = 8.1 msec, flip angle = 8°, slice number = 36, field of view = 240 mm, voxel size = 1 × 1 × 1 mm, matrix size 240 × 240).

Preprocessing of MRI data were completed using SPM8. For each participant, head movements were estimated by realigning each scan to match the first scan in the scanning sequence. Images were normalized and registered to a standard template within SPM (the MNI space) during which functional volume images were resampled to a spatial resolution of 3 × 3 × 3 mm. Low-frequency temporal drifts were removed from the BOLD data using a 1/128 Hz high-pass filter. The global signal was removed by dividing each voxel with the mean value across slices. Images were smoothed using a Gaussian kernel with a FWHM of 6 mm.

BOLD Analysis

Two separate general linear models (GLMs) with parametric modulation were constructed. The first GLM aimed to model the ssVEP-BOLD coupling over the entire experiment. Thus, all trials were modeled in each experimental block separately using a GLM, which consisted of a sequence of boxcar functions in which the start was synchronized with the onset of each stimulus and width equal to the duration of each trial. Each boxcar function was then convolved with a canonical hemodynamic boxcar function. For the second regressor, the height of the boxcar function varied according to the normalized single-trial ssVEP amplitudes. Six additional regressors describing participants' head movements, as determined during preprocessing, were added to this design matrix to account for head movements during the scanning process. This process was repeated for each experimental block, resulting in six task-related regressors, three of which modeled ssVEP-BOLD coupling.

The second model aimed to investigate differences between CS types for both BOLD alone and ssVEP-BOLD coupling across the duration of all experimental blocks. Construction of this model followed the same steps as in the first model but constructed separate regressors for each condition and half within in each block. A CS+ versus CS− contrast was conducted using regressors modeling only the stimulus onsets and durations, resulting in three t maps for each participant representing the extent to which the BOLD activity alone differed between CS types. Whereas the EEG and HR condition differences were assessed by binning trials based on the three experimental phases described above, the BOLD analysis compared CS+ and CS− conditions specifically during the acquisition block to reduce design complexity, to replicate the contrasts available from most previous studies of fear-conditioning, and to enable comparison with extant meta-analyses (Fullana et al., 2016). The same CS+ versus CS− contrast was conducted using ssVEP informed regressors to determine whether ssVEP-BOLD coupling differed between the stimulus conditions.

Single-subject statistical t maps were submitted to a second-level analysis using random-effects models, which examines the extent to which effects reproduce across subjects. Determining significant activation while protecting against false-positives was achieved using cluster-extent based thresholding according to guidelines outlined by Woo, Krishnan, and Wager (2014). Here, a threshold for statistical significance was determined using a cluster-based approach in a two-step procedure: First a minimum voxel-wise threshold ($p < .001$, uncorrected) was applied to identify candidate voxels, and then a second cluster-wise (extent) threshold (FWE $p < .05$) was calculated based on Gaussian Random Field theory (Hayasaka & Nichols, 2003; Friston, Worsley, Frackowiak, Mazziotta, & Evans, 1994). Note that this procedure led to an expected rate of about 5% false-positives in a recent analysis of potentially problematic fMRI analysis methods (Eklund, Nichols, & Knutsson, 2016). Here, a cluster-wise threshold of $k = 14$ was determined. The threshold for the ssVEP-BOLD coupling analyses followed the same steps but used a lower initial voxel-wise threshold ($p < .01$) to account for the reduced variability involved in modeling the residual BOLD activity, which is in line with previous studies using EEG-informed BOLD analyses (Liu, Huang,

McGinnis-Deweese, Keil, & Ding, 2012; Scheeringa, Mazaheri, Bojak, Norris, & Kleinschmidt, 2011; Bénar et al., 2007; Debener et al., 2005; Eichele et al., 2005) and led to a cluster-extent threshold of $k = 23$ voxels. Note that the ssVEP-BOLD analysis sought convergent validity with BOLD-alone and BOLD connectivity analyses, thus providing additional protection against false-positives.

Labeling of significant clusters was conducted using the probabilistic cytoarchitectonic labeling system (Eickhoff et al., 2005) SPM toolbox. The atlas included in this toolbox is constructed based on histological labeling from 10 postmortem brains and includes probabilistic labeling based on interindividual variability of spatial locations, including several areas within visual cortical, hippocampal, and thalamic regions. Visual structures included areas V1, V2, the dorsal and ventral portions of V3 (V3d, V3v) and V4 (V4d, V4v), V5/MT+ (hOC5), four subregions in the fusiform gyrus (FG1, FG2, FG3, FG4), anterior and posterior portions of the lateral occipital cortex (hOC4la, hOC4lp), as well as dorsal and ventral portions of visual extrastriate cortices (hOC3d, hOC4vd, hOC3v, hOC4v). Additionally, this atlas includes subregions within the superior parietal cortex (5L, 5M, 5Ci, 7A, 7PC, 7M, 7P), inferior parietal (PFop, PFt, PF, PFm, PFcm, PGa, PGp), intraparietal sulcus (hlP1, hlP2, hlP3), and parietal operculum (OP1, OP2, OP3, OP4). All hippocampal regions are included in this atlas (DG, CA1, CA2, CA3, CA4, subiculum), and thalamic regions are divided into separate regions based on cortical connectivity as determined by Behrens et al. (2003). Because the histological labeling atlas does not include many anterior cortical structures, clusters located outside the visual cortical, hippocampal, and thalamic regions were labeled using a macroscopic level atlas included in this same toolbox.

HR-BOLD Coupling

One note of caution regarding the use of parametric modulation analyses with BOLD data includes the possibility of spurious results in cases where the parametric modulator systematically reflects pronounced physiological changes such as heart rate or respiration, which directly impact CBF and the BOLD signal (Liu, 2016; de Munck et al., 2008; Wise, Ide, Poulin, & Tracey, 2004). The simultaneous collection of heart rate allowed us to explore the extent to which ssVEP-BOLD coupling was a mere epiphenomenon of the known covariation of ssVEPs with heart rate orienting and cardiac fear acceleration responses (e.g., Keil et al., 2010). Toward this goal, we calculated the maximum change in BPM from baseline 1000 to 4000 msec following stimulus onset for each single trial. These values were used to construct a predictive model for the BOLD activity according to the same methods described in the ssVEP-BOLD coupling analysis methods, including identical voxel-wise ($t = 2.62$) and cluster-extent ($k = 14$) thresholding to guard against false-positives.

Dynamic Causal Modeling

DCM (Friston, Harrison, & Penny, 2003) uses Bayesian modeling to compare possible directional connectivity configurations among brain regions for individual stimulus conditions interleaved within a BOLD time-series and was conducted in the current study as a follow-up analysis to explore networks of brain structures that may give rise to enhanced CS+ activity in visual cortical regions. Specifically, this analysis aimed at characterizing the direction of CS+ BOLD increases relative to visual cortex: whether visual cortical activity enhances activity of extravisual regions (Feedforward), whether any extravisual regions enhance visual cortical activity (Feedback), or if the enhancement is reciprocal in nature (Reciprocal). Toward this aim, we included all regions that demonstrated CS+ relative to CS− BOLD enhancement for both the BOLD-alone and ssVEP-BOLD coupling analyses in a set of connectivity architectures, which modeled all possible directions of CS+ enhanced influence between visual and extravisual regions and tested whether feedback, feedforward, or reciprocal models best described CS+ enhancement. In addition, the bilateral amygdaloid complexes were included as possible structures. Because this analysis was focused on the mechanisms underlying CS+ enhancement, only BOLD data from the acquisition block were submitted to this analysis.

RESULTS

Heart Rate

Heart rate deceleration between 0 and 3000 msec following stimulus onset for both CS+ and CS− in each of the three conditioning phases are illustrated in Figure 2 (bottom) As expected, follow-up t tests between CS types for each of the three phases (preconditioning, postconditioning, postextinction) separately indicated heart rate deceleration was larger for CS+ relative to CS− stimuli during the second phase (postconditioning) only ($t(1, 14) = 2.569, p < .05$).

SAM Ratings

Statistical analysis (paired t test) of the emotional hedonic and arousal ratings obtained at the conclusion of all three experimental sessions revealed no difference between CSs on both arousal (means: CS+ = 5.73, CS− = 5.46; $t(14) = 0.638, p > .05$) and valence (means: CS+ = 4.40, CS− = 4.80; $t(14) = -.764, p > .05$).

EEG-ssVEP

Mean values of ssVEP amplitudes by bins are shown in Figure 2. This figure illustrates a sustained increase in ssVEP amplitude for CS+ relative to CS− trials beginning in the first half of the acquisition block and lasting through the first half of extinction, which is followed by

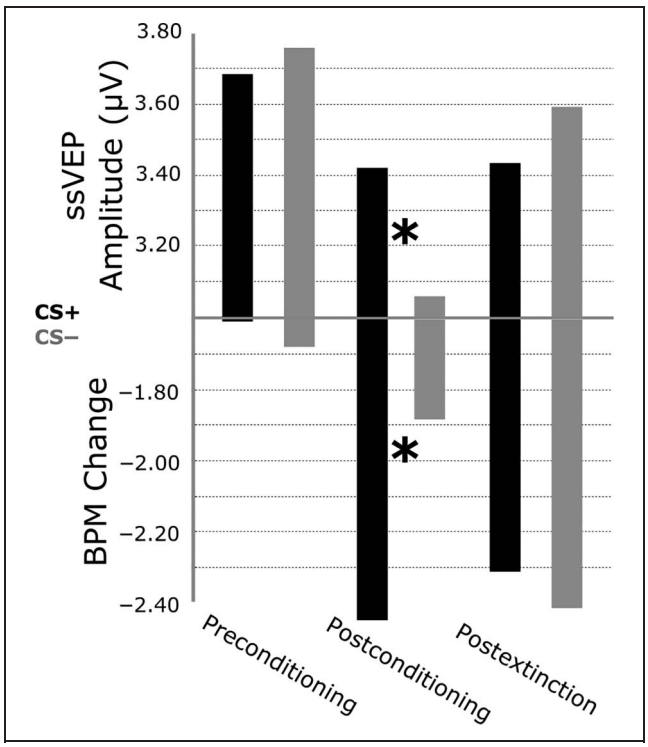

Figure 2. Mean values of both ssVEP amplitudes from sensors Oz (top) and changes in heart rate reactivity (BPM; bottom), for all three phases of the experiment separately. CS+ relative to CS− stimuli showed both greater ssVEP amplitudes and greater deceleration in BPMs during the second phase. For ssVEP amplitudes, a CS × Phase interaction and a CS × Phase quadratic effect were observed.

an increase in CS− relative to CS+ amplitude for the last half of extinction. As expected, t tests comparing CS types for each phase separately showed larger CS+ relative to CS− amplitudes ($t(1, 14) = 2.208, p < .05$), only during the postconditioning phase, when contingencies were established.

Hemodynamic Data

CS+ versus CS−

Cluster locations for all BOLD-alone analyses are shown in Table 1. BOLD activity was greater for CS+ relative to CS− trials during the acquisition block in four separate voxel clusters (Figure 3, red). For one cluster ($k = 14$), significant voxels spanned areas V1, V2, V3v, and V4v. The maximum t value ($t = 4.61$) was also located in the right lingual gyrus. According to the probabilistic labeling atlas, this voxel had the largest probability (37%) of being located in V1, followed by V2 (21%) or V3v (18%). Altogether, significant voxels in this cluster spanned areas V1, V2, V3v, and V4v.

Three additional clusters were located outside the visual cortex and not within the cytoarchitectonic atlas. Two of these clusters were each located in the left ($k = 32$, $t = 4.01$) and right ($k = 21$, $t = 3.66$) insula. Another cluster was located in the right superior temporal gyrus ($t = 6.73$, $k = 23$). The same CS+ versus CS− comparisons during habituation and extinction yielded no significant clusters.

ssVEP-BOLD Coupling

Effects of CS Onset

When all trials across all three experimental blocks were considered, single-trial ssVEP amplitude positively related

Table 1. Anatomical Labels of Clusters that Pass Significance Thresholds

Region	*MNI*	*Peak-t*	*k*
BOLD-alone CS+ > CS−			
R S temporal sulcus	60, −25, −2	4.43	23
L insula	−36, 20, 4	4.01	32
R insula	30, 26, −2	3.66	21
R lingual	18, −88, −5	3.52	14
ssVEP-BOLD CS+ > CS−			
L M F gyrus	−45, 41, 16	5.37	43
R calcarine	6, −91, 7	5.11	54
R M F gyrus	48, 44, 16	3.73	40
L I parietal	−54, −46, 37	3.44	27
ssVEP-BOLD All Trials			
R lingual	12, −88, −8	5.26	92
L M occipital gyrus	−15, −97, 1	4.42	37
L I occipital	−45, −67, −11	4.41	31
R rolandic operculum	39, −4, 16	3.94	46
R thalamus[a]	9, −16, −19	4.81	293
L hippocampus	−33, −34, −8	3.10	38
HR-BOLD All Trials			
L putamen	−15, 4, −3	−4.34	40
L ACC	−9, 37, 0	−4.29	75
L postcentral gyrus	−60, −8, 24	4.52	37
L M F gyrus	−39, 49, 18	4.12	53
R postcentral gyrus	57, −8, 27	3.90	27

All analyses used a cluster-extent threshold of $k = 14$. The BOLD-alone analysis used a voxel-wise threshold of $t = 3.42$ whereas both ssVEP-BOLD and HR-BOLD analyses used $t = 2.62$, as described in the Methods section. L = left; R = right; S = superior; I = inferior; M = middle; F = frontal.

[a]Cluster located in the right thalamus includes coverage of right hippocampus.

to BOLD activity in six clusters (Figure 4). Three of these clusters consisted of occipital cortical areas. For one of these occipital clusters, significant voxels spanned right lateralized areas V1, V2, and the ventral portion of area V3 (V3v). The peak t value (5.26) was located in the right lingual gyrus, with maximum probability of being located in V2 (48%) followed by V1 (43%). Two additional visual cortical clusters emerged: One cluster (k = 37) spanned the left lateralized areas of V1, V2, V3v, V3d, and posterior lateral extrastriate visual cortex (hOC4lp). The maximum t value (4.42) was located in the left middle occipital gyrus, with highest probability of being located in area V1 (58%). Another cluster (k = 31) had a maximum t value (4.41) in the defined left inferior occipital gyrus with highest probability of being located in FG2 (31%). This cluster spanned areas FG2, FG4, and the anterior lateral extrastriate visual cortex (hOC4la).

Three clusters were located in thalamic and hippocampal areas. For the hippocampal cluster (k = 38), the maximum t value (3.11) was located in the left hippocampus, with highest probability of being located in the dentate gyrus (38%). This cluster spanned areas DG, CA1, CA2, the subiculum, CA3, and FG3. Finally, one large cluster of voxels related to ssVEP amplitude (k = 295) spanned extended aspects of the thalamus and hippocampal regions DG, CA1, CA2, and CA3. The maximum t value (4.81) for this cluster had the highest probability of being located in the right temporal thalamic region (38%). One additional clusters existed outside the purview of the Jülich probabilistic atlas in cortical and midbrain areas, in the right rolandic operculum (k = 46; t = 3.94).

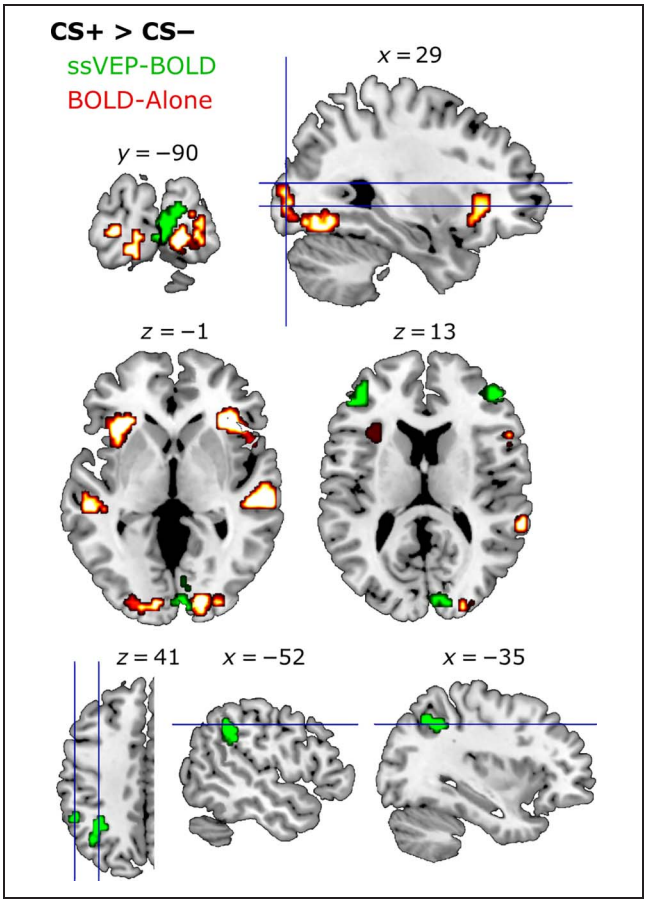

Figure 3. Voxel clusters showing a CS+ > CS− effect in the acquisition block for the BOLD-only (red) and the ssVEP-BOLD coupling (green) analyses. Clusters reported in Table 1 passed are significant when exceeding both a voxel-wise threshold of t = 3.43 and cluster-extent threshold of k = 14 for the BOLD-only analysis, whereas the ssVEP-BOLD analysis used a voxel-wise threshold of t = 2.62 and a cluster extent threshold of k = 23. Clusters illustrated in this figure used less stringent thresholds of t = 2.62 and k = 14 to best illustrate the noise level. MNI coordinates are noted above each corresponding slice.

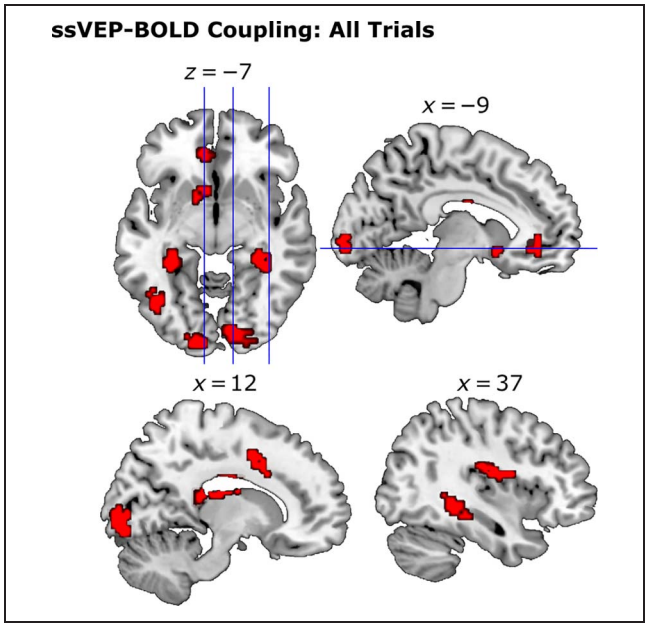

Figure 4. Group level BOLD clusters across 15 participants for ssVEP-BOLD coupling across all trials. To appropriately illustrate the level of noise, clusters shown here pass a voxel-wise threshold of t = 2.62 and a cluster-extent threshold of k = 14, whereas the clusters reported in Table 1 pass more stringent cluster-extent threshold of k = 23. MNI coordinates are noted above each corresponding slice.

Effects of CS+ Compared with CS−

Four clusters of voxels yielded greater ssVEP-BOLD coupling for CS+ relative to CS− trials during acquisition (Figure 3, green; Figure 5). In one cluster (k = 54), the maximum t value (5.11) was located in the right calcarine gyrus. The Jülich probabilistic atlas indicated that this voxel was most likely located in area V1 (46%) but may also be located in area V2 (45%). This cluster spanned area V1 and V2 bilaterally, as well as the right lateralized V3A and V3d.

A second cluster (k = 27) had a maximum t value (3.44) located in the left inferior parietal lobule. This voxel had the highest probability (44%) of being located in the left PFm, spanning the PF, PFcm, hIP2, and PFm.

Two additional clusters were located in frontal regions and outside the regions defined by the cytoarchitectonic atlas. These clusters contained maximum t values the left

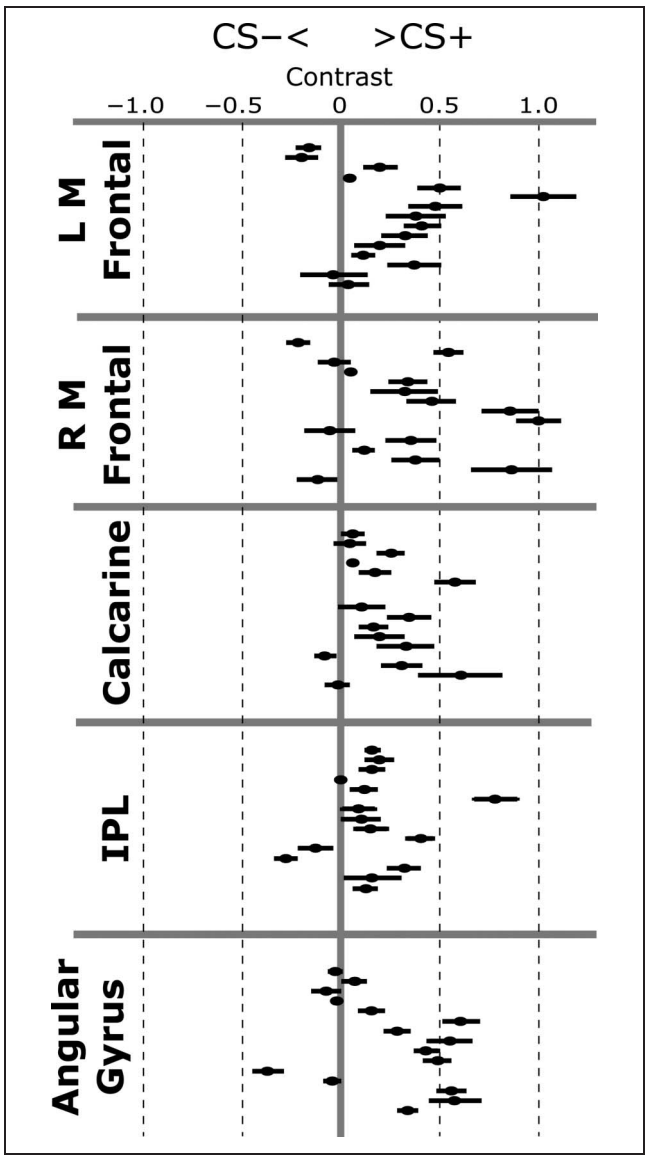

Figure 5. Contrast values for the CS+ minus CS− comparison for ssVEP-BOLD coupling beta values for each of the five significant anatomical clusters, separately for each participant. Data points right of the centerline indicate greater ssVEP-BOLD coupling for CS+ relative to CS− trials. Error bars depict the standard error across all voxels in each ROI.

(k = 43, t = 5.37) and right (k = 40, t = 3.73) middle frontal gyri (MFG).

HR-BOLD Coupling

The complete results of the HR-BOLD coupling analysis can be seen in Figure 6. Two clusters showed significant negative HR-BOLD coupling such that the BOLD signal increased with a larger deceleration (orienting response) of heart rate in response to the CS. One cluster contained a maximum t value (k = 75, t = −4.29) located in the left ACC. The second cluster contained a maximum t value (k = 40, t = −4.34) in the left putamen.

Three clusters showed a positive HR-BOLD coupling, such that the BOLD signal showed greater increase with relative acceleration of the heart. One cluster (k = 53, t = 4.12) was located in the left MFG. Two clusters were located in the left (k = 37, t = 4.52) and right (k = 27, t = 3.90) postcentral gyrus. For the right postcentral gyrus cluster, the probabilistic atlas indicated a 37% probability of this cluster being located in area OP4 of the rolandic operculum. The left postcentral gyrus cluster was assigned a 16.8% likelihood of being located in area 3a of the primary somatosensory cortex and a 12.3% likelihood of being located in area 44 of Broca's region.

Dynamic Causal Modeling

The previous analyses showed an enhanced CS+ BOLD response and ssVEP-BOLD coupling in the occipital pole and calcarine fissure, respectively, as well as multiple structures outside visual areas. An additional question arising from these analyses concerns the dynamics and directionality of communication among these structures during CS+ trials, specifically whether any or all of these extravisual structures (1) modulate the activity in visual cortical clusters (Feedback), (2) are modulated by visual cortical clusters (Feedforward), or (3) share reciprocal modulation with visual cortical clusters (Reciprocal). Toward this aim, the BOLD activity from these regions during the acquisition block was submitted to DCM, which tested the likelihood of multiple possible connection

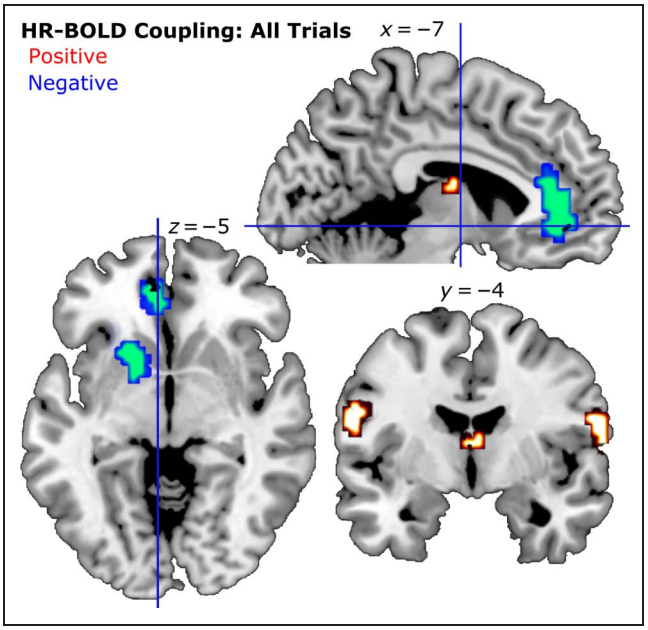

Figure 6. Group level analysis (N = 15) for HR–BOLD coupling across all trials. As in previous figures, clusters shown here pass a voxel-wise threshold of t = 2.62 and a cluster-extent threshold of k = 14. MNI coordinates are noted above each corresponding slice. One cluster near the thalamus shown in this figure largely overlapped with aspects of the third ventricle and thus is not reported here.

models, between the structures identified by BOLD-alone and ssVEP-BOLD analyses. To test whether extravisual regions sent feedback signals to modulate visual cortex, a family of connectivity architectures were constructed to model CS+ influence on the regions in the calcarine fissure and the occipital pole, shown above to be sensitive to conditioned threat. This family of models tested feedback from all extravisual structures together as well as for each region each individually. This process was repeated twice, modeling the connections as feedforward and reciprocal. To test whether these CS+ modulations were exclusive to the occipital pole or calcarine fissure, as opposed to their combination, two additional families of models were constructed as outlined above to model the connection(s) between the occipital pole and calcarine fissure separately. As a result, a total of 63 models were separated into nine families (see Table 2).

The comparison of these nine families revealed that feedback to both the occipital pole and calcarine fissure provided the best characterization of CS+ modulation, yielding a posterior likelihood of 0.77. Models including feedback to the occipital pole alone yielded a posterior likelihood of 0.23. All other model families showed a posterior likelihood of $<2.16 \times 10^{-8}$. A second family comparison was conducted to determine if any specific structures explained CS+ modulation to the occipital pole and calcarine fissure together, as well as the occipital pole alone. Here, each of the seven models (see Table 2) in the occipital pole and calcarine fissure feedback family and the occipital pole feedback family was treated as separate families. This analysis revealed that the right MFG explained this CS+ modulation for both the occipital pole and calcarine fissure, with this model yielding a posterior likelihood of 0.77. The same structure also provided some evidence of CS+ modulation in the occipital pole alone, with a posterior likelihood of 0.23.

Following this analysis, a control was added, comparing connectivity patterns when the effect of safety (CS−) was considered. Thus, an identical set of connectivity architectures was constructed, but modeling CS−-related modulation instead of modulation related to the CS+. The new (CS−) models were then compared family-wise against the CS+ models described above. As expected given that no visuocortical amplification was seen for the CS−, all CS− models displayed a posterior likelihood below 0.05, indicating that CS+ better explained BOLD modulation when compared with CS−.

The amygdala has been widely considered a source of visual cortical feedback, as discussed in the Introduction. However, the BOLD activity in this region did not discriminate between CS type in either the BOLD-alone or ssVEP-BOLD analysis. It has been suggested, however, that CS-type affects amygdala connectivity patterns differently than the local BOLD activity and that both BOLD level and connectivity may change through the course of contingency learning (Bassett, Yang, Wymbs, & Grafton, 2015). Thus, given the prominence of amygdalo-fugal connections in many models of emotional perception, an exploration of models testing the feedback, feedforward, and reciprocal connections between the occipital pole and calcarine fissure and the amygdaloid bodies was conducted. Again, connectivity models including the amygdalae were tested for both CS+ and CS− modulation. These models were submitted to family-based comparisons, which tested (1) whether amygdalo-fugal connections better explained CS+ modulation compared with the original set of connectivity architectures based on brain regions with significant contrasts (above) and (2) whether CS+ or CS− stimuli differentially modulated these connections. These analyses indicated that amygdalo-fugal connections (posterior likelihood = 1.00) better

Table 2. Modeled Connectivity Architectures

Occipital Pole (21 Models)
L insula
R insula
L middle frontal gyrus
R middle frontal gyrus
L inferior parietal lobule
Calcarine fissure
Calcarine Fissure (21 Models)
L insula
R insula
L middle frontal gyrus
R middle frontal gyrus
L inferior parietal lobule
Occipital pole
Occipital Pole + Calcarine Fissure (21 Models)
L insula
R insula
L middle frontal gyrus
R middle frontal gyrus[a]
L inferior parietal lobule

Detail of structures submitted to the DCM analysis, in which modulation of CS+ stimuli between visual cortical structures (italic text) and extravisual structures (nonitalic text) was tested. Specifically, connections were modeled between each of the visual cortical cluster sites and each extravisual region individually as well as all extravisual regions together. These connections were treated as either (1) feedback (visual cortical modulated by extravisual), (2) feedforward (extravisual modulated by visual cortical), or (3) reciprocal (mutual modulation between visual cortical and extravisual).

[a] The DCM analysis indicated that the optimal model was feedback from right MFG to both the occipital pole and calcarine fissure.

explained CS+ modulation compared with the original set of models (posterior likelihood = 5.42×10^{-303}) but reentrant modulation of visual cortex during CS− (posterior likelihood = 0.99) was more strongly supported compared with CS+ trials (posterior likelihood = 5.14×10^{-5}). A follow-up family comparison revealed that CS− (safety) related amygdalo-fugal feedback to the occipital pole was the most strongly supported connectivity pattern among the models including the bilateral amygdala, in which the posterior likelihood was 1.00 whereas all other models did not exceed 0.0003.

DISCUSSION

The current study investigated the large-scale coupling between whole-brain BOLD data and electrophysiologically recorded visual responses (ssVEPs) during classical aversive conditioning. As expected, the ssVEP amplitude, generated in early visual pericalcarine cortical areas, increased for CS+ relative to CS− trials, as participants acquired the CS+ and US contingencies (Gruss, Langaee, & Keil, 2016; Keil et al., 2013; Miskovic & Keil, 2012; Moratti & Keil, 2009; Moratti et al., 2006). Consistent with a large body of hemodynamic neuroimaging research, these differences in visual cortical electrophysiology were accompanied by CS+-specific BOLD activation in visual cortical areas (Klucken et al., 2009; Carter, O'Doherty, Seymour, Koch, & Dolan, 2006; Tabbert, Stark, Kirsch, & Vaitl, 2005; Knight, Cheng, Smith, Stein, & Helmstetter, 2004; Cheng, Knight, Smith, Stein, & Helmstetter, 2003). Importantly, heightened covariation of occipital ssVEP amplitude with BOLD signals was observed in the calcarine cortex, inferior parietal lobule, angular gyrus, and the bilateral MFG, showing greater ssVEP-BOLD coupling when viewing the CS+. No regions displayed greater coupling when viewing the CS−. The robust differential ssVEP-BOLD coupling in the calcarine fissure likely indexes the—well-established—heightened blood flow (e.g., Fullana et al., 2016) and heightened electrocortical responses (Keil et al., 2013) for the CS+ in this same region, thus supporting the validity of the combined ssVEP-BOLD analysis used here.

The temporal covariation among these frontoparietal and occipital structures suggests functional coupling, which may underlie the experience-dependent modulation of activity in the visual cortex. To further examine this question, DCM analyses were conducted. These analyses strongly supported connectivity models in which the selective amplification of visual cortex during threat resulted from cortico-cortical top–down modulation, specifically from the MFG. Evidence for communication between the MFG and visual cortex has long been established as an important component in visual perception and selective attention. For example, frontal lesion studies combined with ERPs (e.g., Barcelo, Suwazono, & Knight, 2000) and neuroimaging studies of selective attention (e.g., Kastner, Pinsk, De Weerd, Desimone, & Ungerleider, 1999) have provided strong evidence that frontal cortex, including the MFG, is involved in selective attention as reflected in changes of visuocortical activity. Large-scale fronto-occipital interactions have also been postulated based on neuroanatomy, with well-known dense white matter tracts connecting MFG to the occipital cortex. Specifically, the bilateral inferior fronto-occipital fasciculi as well as the anterior thalamic radiations may serve as an anatomical means of efficient communication between frontal and occipital structures, either through thalamic relays or directly via the inferior fronto-occipital fasciculi (Forkel et al., 2014). Future work may examine characteristics of these white matter tracts in relation to aversive conditioning.

In a similar vein, it has been extensively demonstrated that BOLD activity in the inferior parietal lobule also found to selectively covary with the ssVEP modulation during threat is sensitive to numerous visual tasks, including changes in directed attention (Corbetta, Kincade, Ollinger, McAvoy, & Shulman, 2000), anticipation of to-be-attended stimuli (Kastner et al., 1999), maintenance of sustained attention (Hopfinger, Buonocore, & Mangun, 2000), and processing of saliency (Clark, Fannon, Lai, Benson, & Bauer, 2000). Deficits in sustained visual attention performance and disrupted visual evoked components follow lesions to these frontoparietal regions (Mizuno et al., 2013; Malhotra, Coulthard, & Husain, 2009; Angelelli, de Luca, & Spinelli, 1996; Lhermitte, Turell, LeBrigand, & Chain, 1985) as well as their inhibition by means of TMS (Lee et al., 2013). Together, the present analyses strongly support a view in which frontoparietal attention networks are the sources of top–down signals, which amplify visual cortical activity during threat perception.

No evidence was observed for a selective influence of deep cortical structures such as the amygdala or anterior insula on visuocortical changes in any of the analyses. Consistent with recent meta-analyses (Fullana et al. 2016), the amygdaloid body did not appear in the BOLD contrast comparing CS+ and CS−. Only about 30% of human fear conditioning studies have reported significant BOLD modulation of the human amygdala (Sehlmeyer et al., 2009). Previous studies have found activation of the amygdala only during the early time course of initial aversive conditioning after which activation reaches a baseline level, ultimately leading to an insignificant activation over the entire time course (LaBar, Gatenby, Gore, LeDoux, & Phelps, 1998). Amygdala activity in the current study also did not covary with the ssVEP amplitude or with modulation of the ssVEP by CS type. Importantly however, connectivity models that included the amygdala showed substantial evidence for reentrant modulation of visual cortex when viewing both CS+ and CS−, with the safety (CS−) condition characterized by greater amygdalo-fugal connectivity, compared with the threat condition. This finding is in line with recent trends in the published literature that deemphasize the selective role of the amygdala in human threat processing (Edmiston et al., 2013), with mounting evidence supporting a view of

the amygdala as involved in a flexible network involved in salience processing (e.g., Markovic, Anderson, & Todd, 2014) and in forming associations of conditioned cues with both threat and safety outcomes (Likhtik & Paz, 2015). Conceptual work has begun to reconcile these findings with a well-documented history of focus on this structure's involvement in fear conditioning in the animal model (Singer, Critchley, & Preuschoff, 2009; Stein, Simmons, Feinstein, & Paulus, 2007; Phelps & LeDoux, 2005; LeDoux, 2003; LaBar et al., 1998; Davis, 1997; Maren & Fanselow, 1996).

When considering all trials across the three experimental blocks, irrespective of CS type, the ssVEP amplitude covaried with BOLD activity in primary visual cortical areas bilaterally and in extended visual occipital, parietal, and anterior cortical sites as well as the thalamus and the hippocampus. These regions are dissociable from MFG, and the inferior parietal sites observed in the CS+ > CS− ssVEP-BOLD coupling analysis were discussed above.

As mentioned in the Methods, one concern regarding parametric modulation analyses of BOLD and autonomic measures has been the susceptibility of these analyses to spurious effects of covariation reflecting overall blood flow, rather than brain-specific activity. Previous studies have addressed this potential physiological contamination by using HR measurements as a nuisance regressor (de Munck et al., 2008). However, in light of the known systematic sensitivity of HR, BOLD, and ssVEP to threat processing (Bradley, 2009; Keil et al., 2008), this approach was not implemented here. Instead, we provided a separate analysis of HR-BOLD coupling, which allows to consider the overlap between ssVEP-BOLD and HR-BOLD. This analysis revealed ACC and putamen covariation with greater decreases in HR, another marker of a threat cue orienting response. This control analysis suggests that ACC and putamen—also observed in the ssVEP-BOLD coupling analysis—may be involved in modulating heart rate or in coordinating a broader cascade of defensive physiological responses, which may include visuocortical tuning and heart rate changes. The remaining ssVEP-BOLD clusters not shared with the HR-BOLD coupling analysis are likely more uniquely involved in modulating visual cortical responses. This potential dissociable nature of multiple brain region functions with regard to threat cue orienting response warrant further exploration and is ideally suited to be studied using multimodal approaches similar to this study.

The ssVEP-BOLD coupling analyses suggest that distinct brain regions communicate with visual cortex at different times, depending on the experimental task, the context, and the significance of the stimulus. This interpretation is consistent with theoretical notions suggesting that visual biases toward threat cues are driven by a subset of the complex, parallel circuits mediating visual processing in distributed brain regions (Pessoa & Adolphs, 2010). Supporting this notion, the present data are inconsistent with a mechanism in which bias signaling is mediated by an isolated brain region such as the amygdala and/or insula.

In addition to visual cortex, the hemodynamic analyses comparing BOLD for CS+ and CS− revealed activation in the bilateral anterior insulae and the right superior temporal cortex. The superior temporal cortex has been reported in several previous neuroimaging studies on aversive conditioning (Straube, Weiss, Mentzel, & Miltner, 2007; Knight, Nguyen, & Bandettini, 2005; LaBar et al., 1998), and a recent meta-analysis found the anterior insulae to be consistently active across the contemporary neuroimaging literature (Fullana et al., 2016). The CS-type difference in these regions did not appear in the ssVEP-BOLD coupling analysis, indicating that electrocortical fluctuations in visual areas did not explain BOLD variance within the aforementioned brain regions. These results suggest that the role of the anterior insula and the superior temporal cortex in aversive conditioning does not involve communication with primary visual cortical regions, at least not on a trial-by-trial basis. Either or both of these regions may be involved in more general visual associative processes, however, or in signaling another defensive physiological response associated with aversive conditioning. Such defensive reactivity was reflected in this study by greater heart rate deceleration for the CS+, compared with the CS− after conditioning (Moratti & Keil, 2005; Hamm & Vaitl, 1996; Hodes, Cook, & Lang, 1985).

A typical finding in delayed classical aversive conditioning is that association formation does not depend on awareness of the CS–US contingency (Clark, Manns, & Squire, 2002). Specifically, metrics of visual cortical engagement (Moratti et al., 2006) and the startle response (Sevenster, Beckers, & Kindt, 2014) show reliable discrimination across a wide range of delayed classical conditioning paradigms in participants with and without reportable insight into the pairing between CS and US. It has also been commonly found that—despite showing conditioning effects—less than half of the participants tend to show measurable evidence of contingency awareness in most classical aversive conditioning studies (Clark et al., 2002). In this study, we used SAM ratings to assess the extent to which participants showed reportable contingency awareness, which perhaps not surprisingly indicated that, as a group, there was no evidence of awareness. The present sample was also limited in size, preventing us from comparing subgroups with and without awareness, which may be a productive avenue for future research.

To conclude, this study combined the temporally sensitive EEG recordings of evoked oscillations generated in pericalcarine cortex with concurrently recorded fMRI. It was found that activity in frontoparietal regions was functionally related to electrocortical activity in pericalcarine areas of the brain and that this coupling was greater when viewing conditioned threat signals. Analyses of directional influence suggest that frontal cortical regions prompt the selective CS+ amplification in visual cortical

areas following CS–US pairing, which serves the function of signaling visual danger cues. Our findings deviate from some of the dominant hypotheses in the field and provide strong evidence that a major component of selective threat amplification occurs via cortico-cortical feedback mechanisms. Future studies may investigate more precisely the spatial and temporal dynamics of the interactions among these regions and whether additional structures not captured by BOLD may mediate their interaction, including whether visual cortical feedback is reentrant or perhaps exist before stimulus onset, reflective of prediction signals acquired over the course of the learning regimen.

Acknowledgments

This research was supported by grants from the National Institutes of Health (R01MH097320) and the Office of Naval Research (N00014-14-1-0542). The authors are grateful to Hong Ji for her assistance with exploring approaches to data analysis.

Reprint requests should be sent to Nathan M. Petro, Department of Psychology, Center for the Study of Emotion and Attention, University of Florida, P.O. Box 112766, Gainesville, FL 32611, or via e-mail: npetro@ufl.edu.

REFERENCES

Allen, P. J., Josephs, O., & Turner, R. (2000). A method for removing imaging artifact from continuous EEG recorded during functional MRI. *Neuroimage, 12,* 230–239.

Allen, P. J., Polizzi, G., Krakow, K., Fish, D. R., & Lemieux, L. (1998). Identification of EEG events in the MR scanner: The problem of pulse artifact and a method for its subtraction. *Neuroimage, 8,* 229–239.

Amaral, D. G. (2003). The amygdala, social behavior, and danger detection. *Annals of the New York Academy of Sciences, 1000,* 337–347.

Amaral, D. G., Behniea, H., & Kelly, J. L. (2003). Topographic organization of projections from the amygdala to the visual cortex in the macaque monkey. *Neuroscience, 118,* 1099–1120.

Anderson, A. K. (2005). Affective influences on the attentional dynamics supporting awareness. *Journal of Experimental Psychology: General, 134,* 258–281.

Angelelli, P., de Luca, M., & Spinelli, D. (1996). Early visual processing in neglect patients: A study with steady-state VEPs. *Neuropsychologia, 34,* 1151–1157.

Barcelo, F., Suwazono, S., & Knight, R. T. (2000). Prefrontal modulation of visual processing in humans. *Nature Neuroscience, 3,* 399–403.

Bassett, D. S., Yang, M., Wymbs, N. F., & Grafton, S. T. (2015). Learning-induced autonomy of sensorimotor systems. *Nature Neuroscience, 18,* 744–751.

Behrens, T. E. J., Johansen-Berg, H., Woolrich, M. W., Smith, S. M., Wheeler-Kingshott, C. A. M., Boulby, P. A., et al. (2003). Non-invasive mapping of connections between human thalamus and cortex using diffusion imaging. *Nature Neuroscience, 6,* 750–757.

Bénar, C.-G., Schön, D., Grimault, S., Nazarian, B., Burle, B., Roth, M., et al. (2007). Single-trial analysis of oddball event-related potentials in simultaneous EEG-fMRI. *Human Brain Mapping, 28,* 602–613.

Bradley, M. M. (2009). Natural selective attention: Orienting and emotion. *Psychophysiology, 46,* 1–11.

Bradley, M. M., & Lang, P. J. (1994). Measuring emotion: The self-assessment manikin and the semantic differential. *Journal of Behavior Therapy and Experimental Psychiatry, 25,* 49–59.

Carter, R. M., O'Doherty, J. P., Seymour, B., Koch, C., & Dolan, R. J. (2006). Contingency awareness in human aversive conditioning involves the middle frontal gyrus. *Neuroimage, 29,* 1007–1012.

Cheng, D. T., Knight, D. C., Smith, C. N., Stein, E. A., & Helmstetter, F. J. (2003). Functional MRI of human amygdala activity during Pavlovian fear conditioning: Stimulus processing versus response expression. *Behavioral Neuroscience, 117,* 3–10.

Clark, R. E., Manns, J. R., & Squire, L. R. (2002). Classical conditioning, awareness, and brain systems. *Trends in Cognitive Sciences, 6,* 524–531.

Clark, V. P., Fannon, S., Lai, S., Benson, R., & Bauer, L. (2000). Responses to rare visual target and distractor stimuli using event-related fMRI. *Journal of Neurophysiology, 83,* 3133–3139.

Clugnet, M. C., & LeDoux, J. E. (1990). Synaptic plasticity in fear conditioning circuits: Induction of LTP in the lateral nucleus of the amygdala by stimulation of the medial geniculate body. *Journal of Neuroscience, 10,* 2818–2824.

Corbetta, M., Kincade, J. M., Ollinger, J. M., McAvoy, M. P., & Shulman, G. L. (2000). Voluntary orienting is dissociated from target detection in human posterior parietal cortex. *Nature Neuroscience, 3,* 292–297.

Cronbach, L. J. (1947). Test "reliability": Its meaning and determination. *Psychometrika, 12,* 1–16.

Damaraju, E., Huang, Y.-M., Barrett, L. F., & Pessoa, L. (2009). Affective learning enhances activity and functional connectivity in early visual cortex. *Neuropsychologia, 47,* 2480–2487.

Davis, M. (1997). Neurobiology of fear responses: The role of the amygdala. *Journal of Neuropsychiatry and Clinical Neurosciences, 9,* 382–402.

de Munck, J. C., Gonçalves, S. I., Faes, T. J. C., Kuijer, J. P. A., Pouwels, P. J. W., Heethaar, R. M., et al. (2008). A study of the brain's resting state based on alpha band power, heart rate and fMRI. *Neuroimage, 42,* 112–121.

Debener, S., Ullsperger, M., Siegel, M., Fiehler, K., von Cramon, D. Y., & Engel, A. K. (2005). Trial-by-trial coupling of concurrent electroencephalogram and functional magnetic resonance imaging identifies the dynamics of performance monitoring. *Journal of Neuroscience, 25,* 11730–11737.

Delgado, M. R., Olsson, A., & Phelps, E. A. (2006). Extending animal models of fear conditioning to humans. *Biological Psychology, 73,* 39–48.

Delorme, A., & Makeig, S. (2004). EEGLAB: An open source toolbox for analysis of single-trial EEG dynamics including independent component analysis. *Journal of Neuroscience Methods, 134,* 9–21.

Di Russo, F., Pitzalis, S., Aprile, T., Spitoni, G., Patria, F., Stella, A., et al. (2007). Spatiotemporal analysis of the cortical sources of the steady-state visual evoked potential. *Human Brain Mapping, 28,* 323–334.

Edmiston, E. K., McHugo, M., Dukic, M. S., Smith, S. D., Abou-Khalil, B., Eggers, E., et al. (2013). Enhanced visual cortical activation for emotional stimuli is preserved in patients with unilateral amygdala resection. *Journal of Neuroscience, 33,* 11023–11031.

Eichele, T., Specht, K., Moosmann, M., Jongsma, M. L. A., Quiroga, R. Q., Nordby, H., et al. (2005). Assessing the spatiotemporal evolution of neuronal activation with single-trial event-related potentials and functional MRI. *Proceedings of the National Academy of Sciences, U.S.A., 102,* 17798–17803.

Eickhoff, S. B., Stephan, K. E., Mohlberg, H., Grefkes, C., Fink, G. R., Amunts, K., et al. (2005). A new SPM toolbox for combining probabilistic cytoarchitectonic maps and functional imaging data. *Neuroimage, 25,* 1325–1335.
Eklund, A., Nichols, T. E., & Knutsson, H. (2016). Cluster failure: Why fMRI inferences for spatial extent have inflated false-positive rates. *Proceedings of the National Academy of Sciences, U.S.A., 113,* 7900–7905.
Forkel, S. J., Thiebaut de Schotten, M., Kawadler, J. M., Dell'Acqua, F., Danek, A., & Catani, M. (2014). The anatomy of fronto-occipital connections from early blunt dissections to contemporary tractography. *Cortex, 56,* 73–84.
Friston, K. J., Harrison, L., & Penny, W. (2003). Dynamic causal modelling. *Neuroimage, 19,* 1273–1302.
Friston, K. J., Worsley, K. J., Frackowiak, R. S. J., Mazziotta, J. C., & Evans, A. C. (1994). Assessing the significance of focal activations using their spatial extent. *Human Brain Mapping, 1,* 210–220.
Fullana, M. A., Harrison, B. J., Soriano-Mas, C., Vervliet, B., Cardoner, N., Àvila-Parcet, A., et al. (2016). Neural signatures of human fear conditioning: An updated and extended meta-analysis of fMRI studies. *Molecular Psychiatry, 21,* 500–508.
Furl, N., Henson, R. N., Friston, K. J., & Calder, A. J. (2013). Top–down control of visual responses to fear by the amygdala. *Journal of Neuroscience, 33,* 17435–17443.
Gallant, J. L., Connor, C. E., & Van Essen, D. C. (1998). Neural activity in areas V1, V2 and V4 during free viewing of natural scenes compared to controlled viewing. *NeuroReport, 9,* 85–90.
Graham, F. K. (1978). Constraints on measuring heart rate and period sequentially through real and cardiac time. *Psychophysiology, 15,* 492–495.
Gruss, L. F., Langaee, T., & Keil, A. (2016). The role of the COMT val158met polymorphism in mediating aversive learning in visual cortex. *Neuroimage, 125,* 633–642.
Hamm, A. O., & Vaitl, D. (1996). Affective learning: Awareness and aversion. *Psychophysiology, 33,* 698–710.
Hayasaka, S., & Nichols, T. E. (2003). Validating cluster size inference: Random field and permutation methods. *Neuroimage, 20,* 2343–2356.
Headley, D. B., & Weinberger, N. M. (2011). Gamma-band activation predicts both associative memory and cortical plasticity. *Journal of Neuroscience, 31,* 12748–12758.
Hodes, R. L., Cook, E. W., III, & Lang, P. J. (1985). Individual differences in autonomic response: Conditioned association or conditioned fear? *Psychophysiology, 22,* 545–560.
Hopfinger, J. B., Buonocore, M. H., & Mangun, G. R. (2000). The neural mechanisms of top–down attentional control. *Nature Neuroscience, 3,* 284–291.
Kastner, S., Pinsk, M. A., De Weerd, P., Desimone, R., & Ungerleider, L. G. (1999). Increased activity in human visual cortex during directed attention in the absence of visual stimulation. *Neuron, 22,* 751–761.
Keil, A., Bradley, M. M., Ihssen, N., Heim, S., Villa, J., Guerra, P., et al. (2010). Defensive engagement and perceptual enhancement. *Neuropsychologia, 48,* 3580–3584.
Keil, A., Miskovic, V., Gray, M. J., & Martinovic, J. (2013). Luminance, but not chromatic visual pathways, mediate amplification of conditioned danger signals in human visual cortex. *The European Journal of Neuroscience, 38,* 3356–3362.
Keil, A., Sabatinelli, D., Ding, M., Lang, P. J., Ihssen, N., & Heim, S. (2009). Re-entrant projections modulate visual cortex in affective perception: Directional evidence from Granger causality analysis. *Human Brain Mapping, 30,* 532–540.
Keil, A., Smith, J. C., Wangelin, B. C., Sabatinelli, D., Bradley, M. M., & Lang, P. J. (2008). Electrocortical and electrodermal responses covary as a function of emotional arousal: A single-trial analysis. *Psychophysiology, 45,* 516–523.
Klucken, T., Kagerer, S., Schweckendiek, J., Tabbert, K., Vaitl, D., & Stark, R. (2009). Neural, electrodermal and behavioral response patterns in contingency aware and unaware subjects during a picture–picture conditioning paradigm. *Neuroscience, 158,* 721–731.
Knight, D. C., Cheng, D. T., Smith, C. N., Stein, E. A., & Helmstetter, F. J. (2004). Neural substrates mediating human delay and trace fear conditioning. *Journal of Neuroscience, 24,* 218–228.
Knight, D. C., Nguyen, H. T., & Bandettini, P. A. (2005). The role of the human amygdala in the production of conditioned fear responses. *Neuroimage, 26,* 1193–1200.
LaBar, K. S., Gatenby, J. C., Gore, J. C., LeDoux, J. E., & Phelps, E. A. (1998). Human amygdala activation during conditioned fear acquisition and extinction: A mixed-trial fMRI study. *Neuron, 20,* 937–945.
LeDoux, J. (2003). The emotional brain, fear, and the amygdala. *Cellular and Molecular Neurobiology, 23,* 727–738.
Lee, J., Ku, J., Han, K., Park, J., Lee, H., Kim, K. R., et al. (2013). rTMS over bilateral inferior parietal cortex induces decrement of spatial sustained attention. *Frontiers in Human Neuroscience, 7,* 26.
Lhermitte, F., Turell, E., LeBrigand, D., & Chain, F. (1985). Unilateral visual neglect and wave p 300: A study of nine cases with unilateral lesions of the parietal lobes. *Archives of Neurology, 42,* 567–573.
Likhtik, E., & Paz, R. (2015). Amygdala–prefrontal interactions in (mal)adaptive learning. *Trends in Neurosciences, 38,* 158–166.
Linnman, C., Rougemont-Bucking, A., Beucke, J. C., Zeffiro, T. A., & Milad, M. R. (2011). Unconditioned responses and functional fear networks in human classical conditioning. *Behavioural Brain Research, 221,* 237–245.
Liu, T. T. (2016). Noise contributions to the fMRI signal: An overview. *Neuroimage, 143,* 141–151.
Liu, Y., Huang, H., McGinnis-Deweese, M., Keil, A., & Ding, M. (2012). Neural substrate of the late positive potential in emotional processing. *Journal of Neuroscience, 32,* 14563–14572.
Malhotra, P., Coulthard, E. J., & Husain, M. (2009). Role of right posterior parietal cortex in maintaining attention to spatial locations over time. *Brain, 132,* 645–660.
Maren, S., & Fanselow, M. S. (1996). The amygdala and fear conditioning: Has the nut been cracked? *Neuron, 16,* 237–240.
Markovic, J., Anderson, A. K., & Todd, R. M. (2014). Tuning to the significant: Neural and genetic processes underlying affective enhancement of visual perception and memory. *Behavioural Brain Research, 259,* 229–241.
Mayr, E. (1974). Behavior programs and evolutionary strategies. *American Scientist, 62,* 650–659.
McTeague, L. M., Gruss, L. F., & Keil, A. (2015). Aversive learning shapes neuronal orientation tuning in human visual cortex. *Nature Communications, 6,* 7823.
Mirabella, G., Bertini, G., Samengo, I., Kilavik, B. E., Frilli, D., Della Libera, C., et al. (2007). Neurons in area V4 of the macaque translate attended visual features into behaviorally relevant categories. *Neuron, 54,* 303–318.
Miskovic, V., & Keil, A. (2014). Escape from harm: linking affective vision and motor responses during active avoidance. *Social Cognitive and Affective Neuroscience:* doi:10.193/scan/nsu1013.
Mizuno, K., Tsuji, T., Rossetti, Y., Pisella, L., Ohde, H., & Liu, M. (2013). Early visual processing is affected by clinical subtype in patients with unilateral spatial neglect: A magnetoencephalography study. *Frontiers in Human Neuroscience, 7,* 432.

Moratti, S., & Keil, A. (2005). Cortical activation during Pavlovian fear conditioning depends on heart rate response patterns: An MEG study. *Cognitive Brain Research, 25,* 459–471.

Moratti, S., & Keil, A. (2009). Not what you expect: Experience but not expectancy predicts conditioned responses in human visual and supplementary cortex. *Cerebral Cortex, 19,* 2803–2809.

Moratti, S., Keil, A., & Miller, G. A. (2006). Fear but not awareness predicts enhanced sensory processing in fear conditioning. *Psychophysiology, 43,* 216–226.

Moratti, S., Keil, A., & Stolarova, M. (2004). Motivated attention in emotional picture processing is reflected by activity modulation in cortical attention networks. *Neuroimage, 21,* 954–964.

Norcia, A. M., Appelbaum, L. G., Ales, J. M., Cottereau, B. R., & Rossion, B. (2015). The steady-state visual evoked potential in vision research: A review. *Journal of Vision, 15,* 4.

Öhman, A., & Soares, J. J. (1998). Emotional conditioning to masked stimuli: Expectancies for aversive outcomes following nonrecognized fear-relevant stimuli. *Journal of Experimental Psychology: General, 127,* 69–82.

Pessoa, L., & Adolphs, R. (2010). Emotion processing and the amygdala: From a "low road" to "many roads" of evaluating biological significance. *Nature Reviews Neuroscience, 11,* 773–783.

Phelps, E. A., & LeDoux, J. E. (2005). Contributions of the amygdala to emotion processing: From animal models to human behavior. *Neuron, 48,* 175–187.

Sabatinelli, D., Fortune, E. E., Li, Q., Siddiqui, A., Krafft, C., Oliver, W. T., et al. (2011). Emotional perception: Meta-analyses of face and natural scene processing. *Neuroimage, 54,* 2524–2533.

Scheeringa, R., Mazaheri, A., Bojak, I., Norris, D. G., & Kleinschmidt, A. (2011). Modulation of visually evoked cortical fMRI responses by phase of ongoing occipital alpha oscillations. *Journal of Neuroscience, 31,* 3813–3820.

Sears, R. M., Schiff, H. C., & LeDoux, J. E. (2014). Molecular mechanisms of threat learning in the lateral nucleus of the amygdala. *Progress in Molecular Biology and Translational Science, 122,* 263–304.

Sehlmeyer, C., Schöning, S., Zwitserlood, P., Pfleiderer, B., Kircher, T., Arolt, V., et al. (2009). Human fear conditioning and extinction in neuroimaging: A systematic review. *PLoS One, 4,* e5865.

Sevenster, D., Beckers, T., & Kindt, M. (2014). Fear conditioning of SCR but not the startle reflex requires conscious discrimination of threat and safety. *Frontiers in Behavioral Neuroscience, 8,* 32.

Singer, T., Critchley, H. D., & Preuschoff, K. (2009). A common role of insula in feelings, empathy and uncertainty. *Trends in Cognitive Sciences, 13,* 334–340.

Sokolov, E. N. (1963). *Perception and the conditioned reflex*. New York: Macmillan.

Stein, M. B., Simmons, A. N., Feinstein, J. S., & Paulus, M. P. (2007). Increased amygdala and insula activation during emotion processing in anxiety-prone subjects. *The American Journal of Psychiatry, 164,* 318–327.

Stolarova, M., Keil, A., & Moratti, S. (2006). Modulation of the C1 visual event-related component by conditioned stimuli: Evidence for sensory plasticity in early affective perception. *Cerebral Cortex, 16,* 876–887.

Straube, T., Weiss, T., Mentzel, H.-J., & Miltner, W. H. R. (2007). Time course of amygdala activation during aversive conditioning depends on attention. *Neuroimage, 34,* 462–469.

Tabbert, K., Stark, R., Kirsch, P., & Vaitl, D. (2005). Hemodynamic responses of the amygdala, the orbitofrontal cortex and the visual cortex during a fear conditioning paradigm. *International Journal of Psychophysiology, 57,* 15–23.

Todd, R., & Thompson, E. (2015). Strengthening emotion-cognition integration. *Behavioral and Brain Sciences, 38,* e87.

Weinberger, N. M. (2004). Specific long-term memory traces in primary auditory cortex. *Nature Reviews Neuroscience, 5,* 279–290.

Wise, R. G., Ide, K., Poulin, M. J., & Tracey, I. (2004). Resting fluctuations in arterial carbon dioxide induce significant low frequency variations in BOLD signal. *Neuroimage, 21,* 1652–1664.

Woo, C.-W., Krishnan, A., & Wager, T. D. (2014). Cluster-extent based thresholding in fMRI analyses: Pitfalls and recommendations. *Neuroimage, 91,* 412–419.